KTH Industrial Engineering and Management

Design of ablative insulator for solid rocket booster

Simon Westerlund

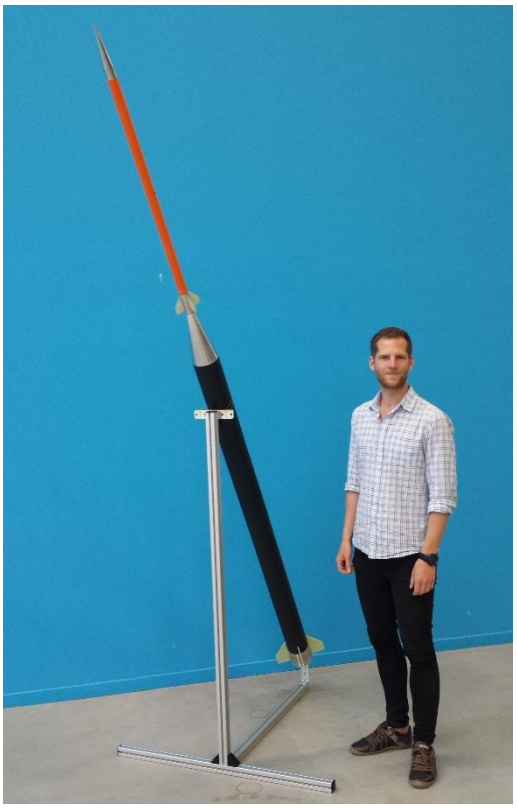

Master of Science Thesis

KTH School of Industrial Engineering and Management
Energy Technology
Stockholm, Sweden

Abstract

The objective of this master thesis was to investigate an ablative liner for the T-Minus DART booster that will accelerate a dart to Mach 5.2 within five seconds. An oxyacetylene torch test was used to sort out the obviously bad materials. Glass fiber/epoxy, with and without alumina as fire retardant, and carbon fiber/epoxy were selected for further investigation. A sub-scale motor was built to expose the materials for conditions similar to the booster conditions in regard to temperature, chemistry, flow velocity and pressure. The target pressure could not be reached in the sub-scale motor but a polynomial function was fitted to the data in order to extrapolate the data and estimate the ablation rate at 7 MPa. The final design is always based on measurements on full scale motors. This could not be done within this report. Recommendation for future work is to use an insulator of 1.8 mm of carbon fiber/epoxy or 1.3 mm of glass fiber/epoxy/alumina for the sub-scale firings to come.

Acknowledgements

I would like to thank Dr. Björn Laumert for being my supervisor during this thesis. He has provided good guidance and been a big help during this project. I'm also thankful to Prof. Nickolay Ivchenko who put me in contact with and recommended me to T-Minus Engineering.
My great gratitude goes to Roel Eerkens, Hein Olthof, Eric Smit and Mark Uitendaal at T-Minus Engineering who has supported me, answered my questions and taught me about solid rocket propulsion like no university in Sweden can.
I also want to thank my parents, Marita and Ewan Westerlund, who always have loved and supported me. Even when I as a 14 year old started to build rockets and since then have caused several fires, explosions and dead spots on the lawn.

Nomenclature

Abbreviations and expressions

AN – Ammonium nitrate

AP – Ammonium perchlorate

APCP – Ammonium perchlorate composite propellant

DART – Dutch Atmospheric Research Tool

FR – Fire Retardant

Klemmung – Area ration between burning propellant surface and nozzle throat

KN – Potassium nitrate

KP – Potassium perchlorate

Symbols

Symbol	Unit	Description
Bi	-	Biot number
c_{gas}	-	Part of the insulator that turns into gas upon pyrolysis
c_p	J/(kg·K)	Specific heat capacity
D	m	Diameter
Fo	-	Fourier number
$h,\ h_g$	W/(m²·K)	Heat transfer coefficient
h_{dest}	J/kg	Enthalpy of destruction
I_{sp}	s	Specific impulse
Lu	-	Luikov number
$M_{combust}$	kg/mol	Mean molecular weight of combustion products
$M_{decompose}$	kg/mol	Mean molecular weight of pyrolysis products
P	Pa	Local pressure
p_c	Pa	Combustion chamber pressure
$Q*$	J/kg	Effective heat of ablation
$\dot{Q}_{conv}$	W/m²	Power of convective heating transfer
$\dot{Q}_{decompose}$	W/m²	Power to decompose insulator
$\dot{Q}_{film}$	W/m²	Power of film cooling
$\dot{Q}_{trans}$	W/m²	Transpiration cooling power
$\dot{Q}_{tot}$	W/m²	Total heat flux
R	m	Radius
Re	-	Reynolds number
T	K	Temperature
t	s	Time
$T_{decompose}$	K	Decompose temperature of insulator
T_{wall}	K	Inside wall temperature of combustion chamber
v	m/s	Local gas/particle velocity
$\dot{x}_a$	m/s	Local ablation rate
x_i	m	Total insulator thickness

Symbol	Unit	Description	Symbol	Unit	Description
α_{wall}	-	Combustion chamber absorptivity	μ	Pa·s	Viscosity
γ	-	Injection coefficient	ρ	kg/m^3	Density
ε_{flow}	-	Flow emissivity	σ_{SB}	kg/(s^3·K^4)	Stefan Boltzmann constant: 5.670373·10^{-8}
ε_{wall}	-	Combustion chamber wall emissivity	χ_i	m^2/s	Thermal diffusivity of insulator
			χ_{cl}	m^2/s	Thermal diffusivity of gas/particle cloud

Table of Contents

1 Introduction

The first scientific sounding rocket Wac Corporal that was launch from White Sands 1945. It was about 5 meters long, equipped with a liquid hypergolic motor and a solid booster and weighed 320 kg. It could lift 11 kg to 64 km altitude. [1] Ever since sounding rockets have been used to reach the parts of the atmosphere that are higher than balloons can reach and lower than satellites can go because of atmospheric drag. Sounding rockets don't go into orbit, they reach a certain altitude and then fall back to earth. This make sounding rockets ideal from atmospheric research, considerable cheaper than satellites and orbital rockets.

There are a variety of rocket propellants as can be seen in figure 1. Rockets may have been used in combat the first time 1232 in China during the war against the Mongol hordes at Kai Feng Fu but ambiguities in the language makes this uncertain. [2] Less controversial is that 1264 fireworks rockets frightened the Empress-Mother Kung Sheng during a feast held in her honor. [3] The rockets used an early version of black powder which later came to consist of 75 % potassium nitrate, 15 % coal, 10 % sulfur.

Modern rockets started in 1926 when Robert Goddard flew the first liquid fueled rocket in Auburn, Massachusetts, where he also used the Swedish invention called de Laval nozzle which accelerates the gases traveling out of the motor. [4] Rocket development made huge progress during the 20th century and different kinds of motors where developed for different kinds of missions. See table 1.

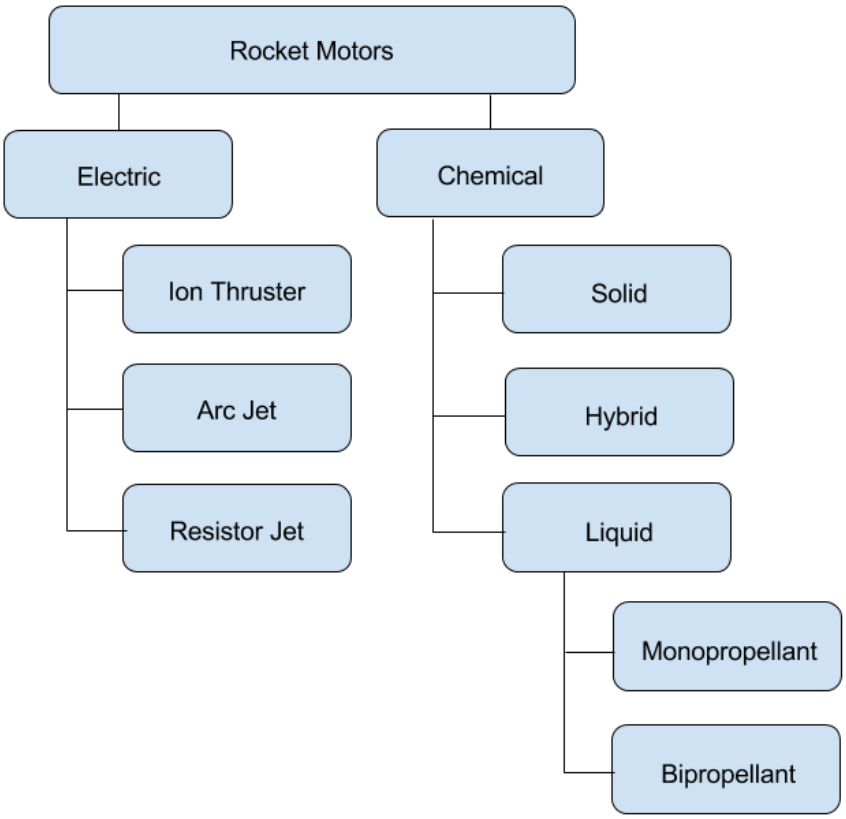

Figure 1. Rocket propellants.

Table 1. Comparison of rocket motors.

Propellant	**Uses**	**Advantage**	**Disadvantage**
Solid	Small launchers, missiles, sounding rockets	Simple, cheap, high power, storability, reliable	Low I_{sp}, difficult to control
Hybrid	Sounding rockets	Safe, controllable	
Monopropellant	Satellite attitude control	Simple	Low I_{sp}
Bipropellant	Launchers, satellite attitude control and orbit raiser	High I_{sp}, high power	Complex, expensive
Ion thruster	Satellite attitude control and orbit raiser	Very high I_{sp}	Very low power
Arc jet	Satellite attitude control	Simple	Very low power
Resistor jet	Satellite attitude control	Very simple	Very low power

No electric thruster has so far been able to lift itself and its power supply from ground which make them unsuitable as sounding rockets. Instead, chemical rockets are used which can produce higher thrust. Solid propellants advanced during and after World War II and made it possible to make big, reliable and efficient motors. [5]

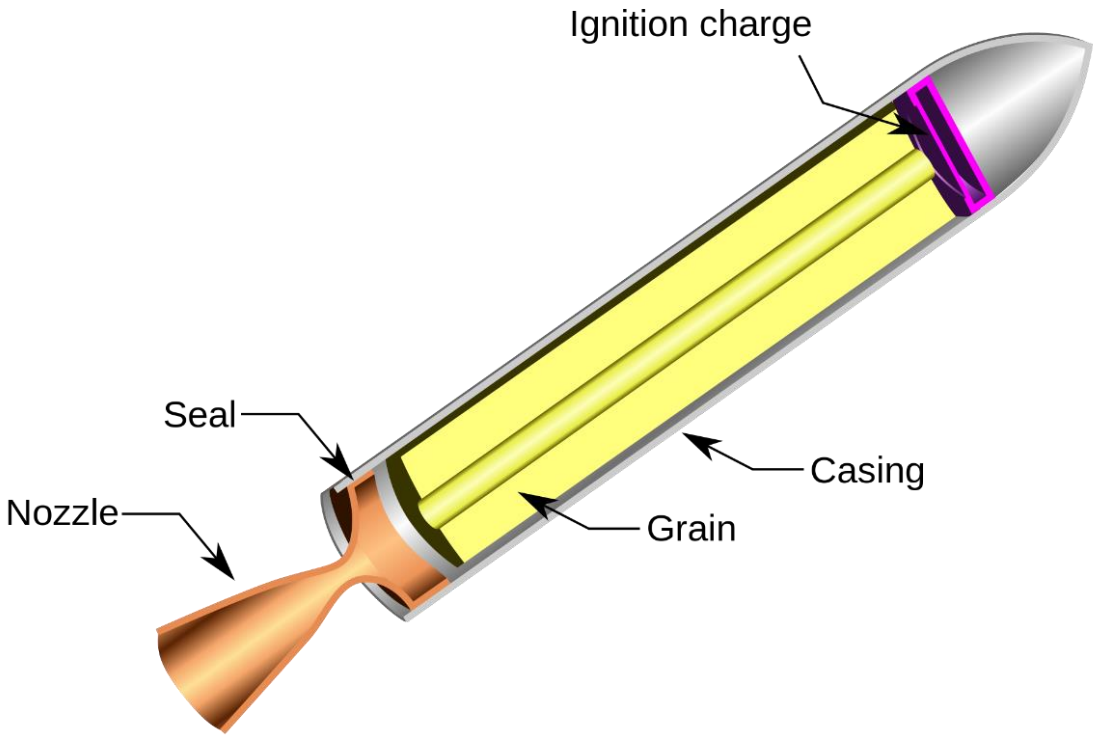

Figure 2. Solid rocket motor.

A solid motor usually consists of a propellant grain bound to the casing. A hole is made through the grain to increase the burn area. See figure 2. The pressure in the motor is set by the area ration between the burning propellant surface and the nozzle throat and every propellant has its own ratio to achieve a certain pressure.

A common type of propellant is composite propellants that usually consists of an oxidizer which has oxygen bound within the molecule and is released when the oxidizer is heated. A metal powder such as aluminium or magnesium is used as fuel and a polymer is added as a binder to the mixture but will also act as fuel. Metals burn very hot but the combustion products are solid or liquid at the combustion temperature which mean that they will heat the rest of the combustion products but not generate any more gas. For this reason the amount of metals in propellants are usually kept below 20 %.

The most common oxidizer is ammonium perchlorate, AP, but ammonium nitrate, AN, potassium perchlorate, KP, and potassium nitrate, KN, are sometime used but with lower performance. [6] A very powerful oxidizer is nitronium perchlorate which unfortunately has turned out to be too unstable to use so far. [7]

The binder's job is to hold the propellant together. Ideally it is a low viscous liquid that during curing becomes a ductile material that can handle mechanical loads and the chemical environment. The minimum amount of binder a propellant must have is to fill the volume between the oxidizer/fuel particles. There is plenty of volume between them if only one particle size would be used. Random packed particles usually fill up 64 % of the volume which require a big amount of binder and the result is a low performance propellant. [8] The empty volume decreases drastically if the oxidizer and fuel consists of several different sizes. See figure 3.

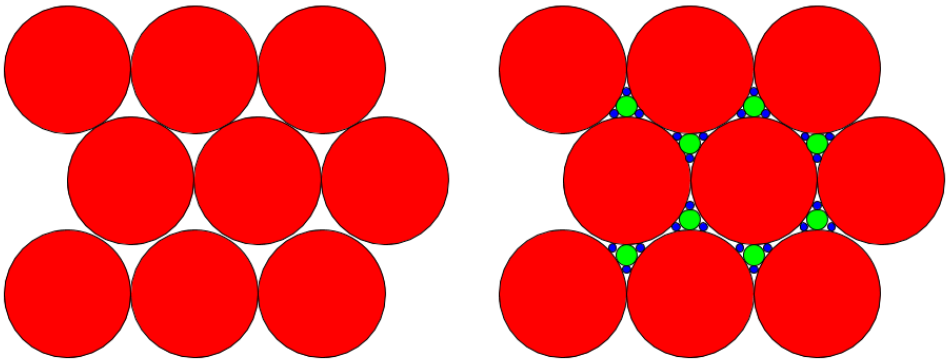

Figure 3. Left: Single size spheres packing in 2D. Right: Multi size spheres packing in 2D.

The shape of the propellant is a vital aspect of solid propulsion. The motor's burn profile can be altered by adjusting the geometry of the fuel. See figure 4. Very common is to use the propellant to protect the combustion chamber walls from the flame since this reduces the amount of insulator needed and gives a lighter structure. The designer also tries to fill up as much of the motor volume as possible to enhance the mass ratio. [9] A common propellant shape in simple engines are cylinders stacked on top of each other with a concentric hole through the grains. The outer diameter is inhibited to burn but the ends and inner diameter are not. By choosing the outer diameter, web thickness and length of the grain carefully one can obtain a quite neutral burn profile and a propellant geometry that is easy to manufacture. This is known as bates grains. [10]

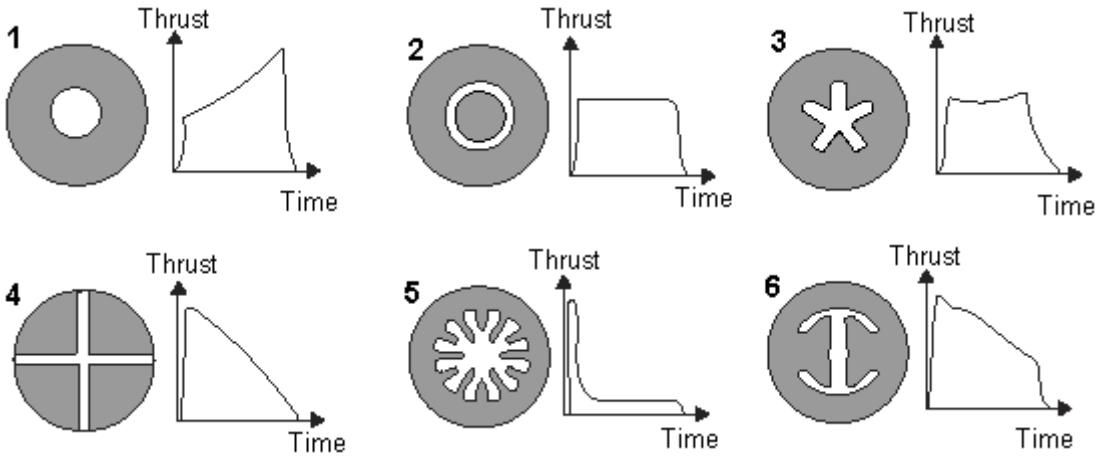

Figure 4. Propellant geometries and burn profiles.

The majority of sounding rockets used today are based on old military discarded motors and their housing equipment. That means that most sounding rockets are old and inefficient for doing science. Some rockets where mass produced during the cold war and the stocks are now running out like the Super Loki. The T-Minus DART system is designed to fill this void. With this low-cost and rapidly deployable rocket system, small payloads can be launched to altitudes above 120 km, from which they can descend through the atmosphere and perform in-situ measurements. The vehicle consists of a lightweight and powerful booster motor and a dart-shaped payload compartment. See figure 5.

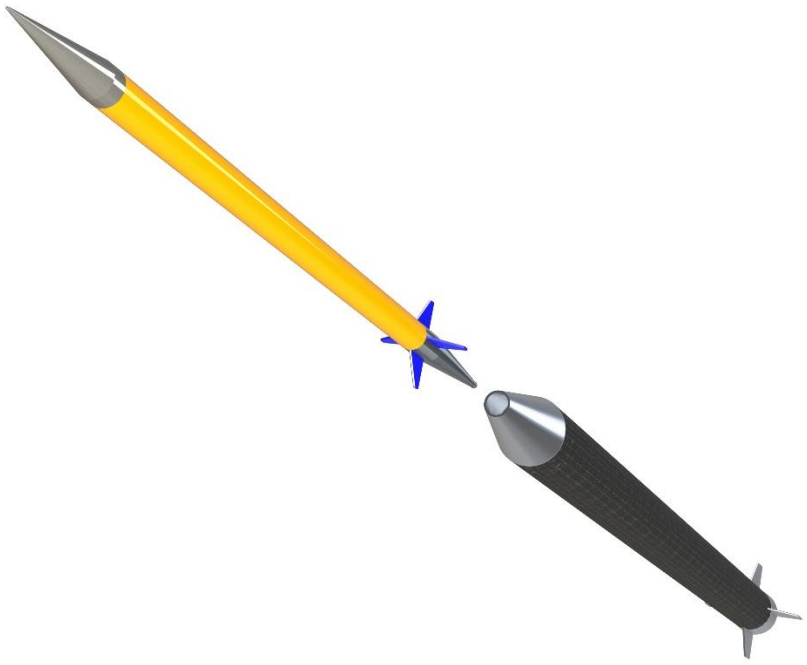

Figure 5: T-Minus DART during separation of booster and dart

The conceptual design of the booster is a lightweight carbon fiber casing and ammonium perchlorate composite propellant (APCP) shaped in a multi-bates grain configuration. Since the carbon fiber uses an epoxy matrix the ability to withstand high temperatures is very limited. Therefor a thermal liner is needed to protect the combustion chamber walls from the heat.

There are several ways of protecting a surface from incoming heat. Liquid fuel engines often uses regenerative cooling by letting the fuel flow through channels in the chamber wall before injected in the combustion chamber. By doing that the heat is transported away from the chamber walls increasing the energy level of the fuel and therefor increasing the specific impulse. This can't be done with solid propellant. [11] See figure 6.

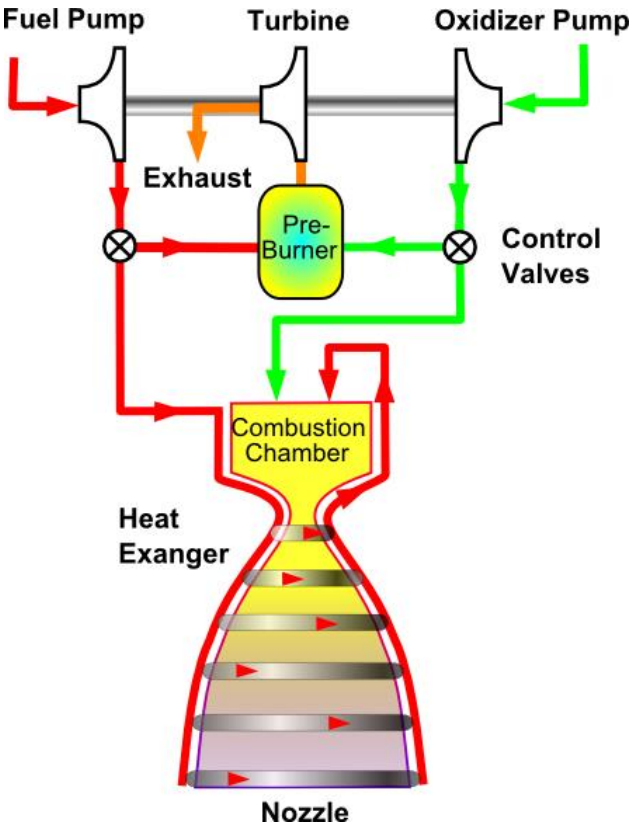

Figure 6. A gas generator cycle engine with generative cooling.

Another way would be to use a material on the inside of the engine that could withstand the heat of the combustion and with sufficiently low thermal conductivity to protect the casing from the heat. This was used in the early days of solid fuel rocketry but has now days often been exchanged for case bound propellants and/or ablative heat protection which will be discussed in this report.

2 Theory

The turbulent, multiphase flow of a solid fuel rocket engine is a very complex environment. The convective heat transfer depends on pressure, chemical composition, flow velocity, temperature and position in the combustion chamber. At operating temperature around 3000 K radiative heat transfer can play a big role but gases does not radiate with a frequency continuum as black bodies but only at certain frequencies. However, solid fuels often contains aluminium for increased specific impulse which produce micron-size alumina particles in the combustion process which is a liquid or a solid depending on the circumstances. The presence of alumina will increase the ability to radiate heat and is dependent on particle size, density and concentration but the optical thickness of this multi-phase flow is very high which means that the major processes will take place near the chamber walls. This effect will gives rice to an intricate phenomenon where higher heat flux can be seen near the front bulkhead in flight engines compared to static fired engines. The motor acceleration makes a buoyancy-induced movement push particles away from the front bulkhead and increases the mean free path locally near the bulkhead resulting in a higher radiative heat flux. [12]

The alumina particles interact with nozzle and combustion chamber walls in several ways. It contributes to convection by liquid alumina collides with the walls and solidifies on the surface transferring heat to the wall. The details of this mechanism are not fully understood. [13]

Mechanical interactions between these particles and walls occur when the flow changes direction. The nozzle, in particular, faces this situation where the particles collide with the nozzle and mechanically erode the surface. [14] These are just some of the challenges that the booster designer faces.

To protect the structural integrity of the booster an insulator of some kind is needed. The most common type is an ablative insulator which provide protection by sacrificing itself. It is widely used for internal rocket motor insulators, nozzles and atmospheric reentry vehicles. The ablator is often made of plastic or rubber reinforced with fibers or particles. When the surface is exposed to heat the insulator starts to decompose, producing gas that forms a protecting boundary layer and the remains of the insulator form char on the surface. The zone of decomposing material travels through the insulator and the generated gas cools the porous char layer on its way to the boundary layer. This lead to a situation where the ablation rate is practically independent of the materials heat conductance. [14] See figure 7.

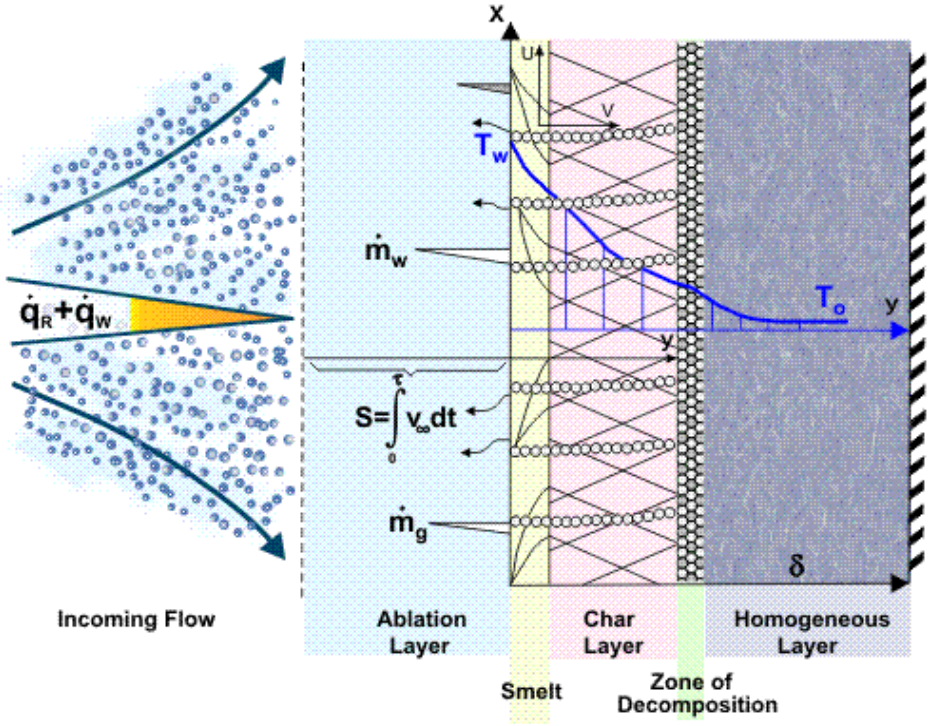

Figure 5: Description of the ablation process

There are a few different mechanisms behind the surface regression.

(1) Chemical effects:

- Surface chemical reaction of char-layer components with propellant gases and particles (usually liquid).
- Subsurface reactions (usually pyrolysis) in the char zone and the decomposition zone.

(2) Physical effects:

- Surface erosion due to particles impingement and shear stress imposed by skin friction.
- Thermal stress induced by heat transfer.
- Subsurface weakening due to mechanical and thermal stresses in the char layer and the decomposition zone; e.g. spallation due to internal pressure created by pyrolysis gas.

(3) Combination of chemical and physical effects. [14]

It is very difficult to consider all these effects individually when designing an ablative insulator. Instead there are three methods that can be utilized. Q* analysis, char-and-erosion-rate analysis and ablation simulation. [14]

2.1 Q* analysis

The Q* method is based on a mathematical simplification of the complicated ablation process. The main assumptions are that the ablation rate is proportional to the total heat flux and that the highest temperature of the insulator is the decomposition temperature. [14]

$$Q^* = \frac{\dot{Q}_{tot}}{\dot{x}_a \rho} \tag{1}$$

Where

Q^* = effective heat of ablation [J/kg]

$\dot{Q}_{tot}$ = total heat flux [W/m^2]

$\dot{x}_a$ = local ablation rate [m/s]

ρ = density [kg/m^3]

Values of Q^* must be determined experimentally or be obtained from literature since the ablation process is not fully understood. When Q^* is known a 1-D heat transfer simulation can be done. This method doesn't consider insulators that form a hard high-temperature char layer that will change the temperature profile significantly.

The Q* method has reasonable results if Q^* is determined under similar conditions for which the new insulator is being designed.

2.2 Char-erosion-rate analysis

The char-erosion-rate method is an empirical method which often are the entire foundation for an insulator design. [14] Measurements from full scale motors can be used or material test samples can be placed in a sub-scale motor and exposed to similar conditions as the target motor and char and erosion rates can be measured meanwhile temperature profiles cannot be studied. When limited data is available a simplified correlation can be expressed as

$$\dot{x}_a = C_1 P^a T^b v^c \tag{2}$$

where

$\dot{x}_a$ = char rate [m/s]

P = local pressure [Pa]

T = temperature [K]

v = local gas/particle velocity [m/s]

C_1, a, b, c = empirical constants fitted to the data for char rate

When more extensive data is at hand another correlation can be used that takes more aspects into account that is believed to be relevant to describe the complex phenomenon of charring and erosion. Since ablation is not fully understood a rigorous mathematical model has not been developed that take all relevant variables into account to an appropriate extent. Instead an equation based on dimensionless groups has been used. [14]

$$Lu = C_2 \,\mathrm{Re}^a \, Fo^b Bi^c \left(\frac{r}{\dot{x}_i} \right)^d \left(\frac{\chi_i}{\chi_{cl}} \right)^e \varepsilon_{cl}^f \tag{3}$$

where

Lu = Luikovnumber = $\dfrac{r\dot{x}_{ch}}{\chi_i}$

Re = Reynolds number = $\dfrac{\rho v r}{\mu}$

Fo = Fourier number = $\dfrac{\chi_i t}{r^2}$

Bi = Biot number = $\dfrac{hr}{k_i}$

r = radius of flow channel (i.e., ½ chamber inner diameter at a given location)

x_i = total insulator thickness

h = overall coefficient of heat transfer from the exhaust gas to the insulator

t = Time

μ = absolute viscosity

χ_i = thermal diffusivity of insulator

χ_{cl} = Thermal diffusivity of gas/particle cloud

C_2, a, b, c, d, e, f = Empirical constants for this equation fitted to the data on Lu

In order to have reliable results extensive data is required from a variety of motors. Small subscale motors to large booster, long and short durations under different pressures. Different insulators, propellants and flow velocities. With a sufficient amount of data one can predict an upper confidence line and make a new design in a way that it will be conservative with a 95 % probability. [14]

This method has proved to be sufficient and an effective way of making a preliminary insulator design. However, it must be emphasized that final designs are always based on measurements on full scale post fired motors.

2.3 Ablation simulation

The most advanced method is the finite-difference boundary-layer/charring-ablator analysis. Mostly it has been used to model ablation for rocket nozzles but the method can be expanded to be valid to insulators as well. [14] The insulator is modeled in three zones. Char and residue zoon, the zone of the pyrolysis process that produce gas that travels through the char zoon and reacts with the propellant flame and the third zoon is the fresh insulator material. See figure 7.

Chemical reactions on the surface between the char layer, pyrolysis gas and the boundary layer gas is taken into account together with heat transfer simulations in the insulator. Mechanical erosion, radiative heat transfer and convective heat transfer are important factors and everything will end up answering the two important questions about surface erosion and temperature distribution within the insulator as a function of time.

3 Simulations

Some initial simulations were made by the means of the Q* method and by ablation simulation slightly different from the method mention above.

3.1 Q* analysis

A Matlab script where done based on the Q* method but no reliable results could be found since it turned out to be very difficult to obtain data about ablation rates for similar insulation materials. The material constant *effective heat of ablation* could not be found but hints from in the literature gave simulation results of 0.2-0.6 mm/s when the total heat flux was set to 1-4 MW/m² and effective heat of ablation was set to 4,1 MJ/kg. The reliability was low and the method was abandoned.

$$\dot{x}_a = \frac{\dot{Q}_{tot}}{\rho Q^*} \tag{4}$$

$\dot{Q}_{tot}$ = total heat flux, Q^* = effective heat of ablation, ρ = density of insulator. [14]

3.2 Ablation simulation

When studying the ablation phenomenon in detail several intricate processes appear. As seen in figure 7 the ablation process is divided in several zones. The incoming heat will cause pyrolysis of the insulator that will produce gas and a char layer on the surface of the insulator. The amount of energy that is required to decompose the insulator is called *enthalpy of destruction* and the process is described by

$$\dot{Q}_{decompose} = \rho \dot{x}_a h_{destruct} \tag{5}$$

Where ρ = insulator density, $h_{destruct}$ = enthalpy of destruction, $\dot{x}_a$ = ablation rate. [15]

How thick the char layer will become is a question about the structural integrity of the char layer, chemical resistance and melting point. The pyrolysis gas percolates through the porous char layer which will act like a heat exchanger. This principle is known as transpiration cooling. [16]

$$\dot{Q}_{trans} = \rho \dot{x}_a c_p c_{gas} (T_{wall} - T_{decompose}) \tag{6}$$

Where c_p is specific heat of pyrolysis products, c_{gas} is how much of that ablator that turns into gas, T_{wall} is temperature of insulator surface, $T_{decompose}$ is decomposition temperature of insulator.

The pyrolysis gas will, according to the theory, have the same temperature as the top char layer when it leave the surface and is injected into the boundary layer where it will act as another heat barrier when it pushes the hot combustion products away. This is known as film cooling. [17]

$$\dot{Q}_{film} = \gamma \dot{x}_a \rho c_p c_{gas} (T_{gas} - T_{wall}) \tag{7}$$

$$\gamma = 0.6 \left(\frac{M_{combust}}{M_{decompose}} \right)^{0.24} \tag{8}$$

$M_{combust}$ = mean molecular weight of combustion products and γ is the injection coefficient.

Convective heat transfer is described by

$$\dot{Q}_{conv} = h_g (T_{gas} - T_{wall}) \tag{9}$$

The heat transfer coefficient, h_g, is complex to model and depends on many variables. Bartz's formula has been around since the 50s. It appears in a few different versions and most companies has their own version which they keep secret. [18]

$$h_g = \frac{0.026}{D_t^{0.2}} \left(\frac{p_c}{C^*} \right)^{0.8} \left(\frac{D_t}{D} \right)^{1.8} c_p \mu^{0.2} \left(\frac{T_{gas}}{\langle T \rangle} \right)^{0.68} \tag{10}$$

Where D_t is the nozzle throat diameter, p_c is the pressure, D is the diameter at the place of interest, $\mu = \mu_{ref} \left(T_{gas} / T_{ref} \right)^{\omega}$ is the viscosity of the combustion gas and $\langle T \rangle$ is described by $(T_{gas} + T_{wh})/2$ where T_{wh} is the estimated wall temperature.

Thermal radiation from the gaseous combustion products tend to be very low since gases radiate only at certain frequencies and not at the whole spectra as black bodies. On the other hand, if the propellant contains metals for increased specific impulse solid and liquid metal oxides will be present in the flow and increase the emissivity according to

$$\varepsilon_{flow} = 1 - e^{(-aQ)} \tag{11}$$

Where *a* is a function of particle size, density and concentration and Q is the mean beam path length. This relationship could not be used to its full extent since a lot of the variables were unknown but according to reference [19] a value of 0.2 were common for small engines with high aluminium content. The thermal radiation is described by

$$\dot{Q}_{rad} = \sigma_{SB} (\alpha_{wall} \varepsilon_{flow} T_{flow}^4 - \varepsilon_{wall} T_{wall}^4) \tag{12}$$

Where σ_{SB} is Stefan-Boltzman's constant and α_{wall} is the absorptivity of the wall. The char layer produced by the ablation often consists of nearly pure graphite which has a high emissivity coefficient and can withstand high temperatures. This can lead to a situation where the net radiation from the wall will be negative.

The heat balance is stated as:

$$\dot{Q}_{conv} + \dot{Q}_{rad} = \dot{Q}_{decompose} + \dot{Q}_{trans} + \dot{Q}_{film} \tag{13}$$

These equations formed a system:

$$\begin{aligned}
\dot{Q}_{decompose} &= \rho \dot{x}_a h_{destruct} \\
\dot{Q}_{trans} &= \rho \dot{x}_a c_p c_{gas} (T_{wall} - T_{decompose}) \\
\dot{Q}_{film} &= \gamma \dot{x}_a \rho c_p c_{gas} (T_{gas} - T_{wall}) \\
\dot{Q}_{conv} &= h_g (T_{gas} - T_{wall}) \\
\dot{Q}_{rad} &= \sigma_{SB} (\alpha_{wall} \varepsilon_{flow} T_{flow}^4 - \varepsilon_{wall} T_{wall}^4) \\
\dot{Q}_{conv} + \dot{Q}_{rad} &= \dot{Q}_{decompose} + \dot{Q}_{trans} + \dot{Q}_{film}
\end{aligned} \tag{14}$$

Where $\dot{Q}_{conv}, \dot{Q}_{rad}, \dot{Q}_{decompose}, \dot{Q}_{trans}, \dot{Q}_{film}, T_{wall}$ and $\dot{x}_a$ are unknown. This gave an equation system with six equations and seven unknowns. No additional equation or reasonable assumption were found and the system could not be solved. A more successful way of simulating the ablation process is to make a full flow and heat transfer simulation of the engine by using Navier-Stokes equations. This is very complicated and the results are still uncertain. "If the char is structurally week, it may be ejected from the surface in the form of large particle chunks, discrete lamina, or as a complete char layer. Therefore, it is very difficult to analyze the thermal, chemical and mechanical behavior of the actual material." [20]

3.3 Simulation conclusions

The ablation process is very complex and not fully understood. Simulations are always based on experimental constants. These constants could not be obtained from literature which made all simulations uncertain. Therefore, two test series were set up to investigate the behavior of the ablation process.

4 Oxyacetylene torch test

The first challenge was to choose which materials that could be used as insulators. In order to sort out obviously bad materials from more interesting once an oxyacetylene torch test was conducted. By exposing materials for a high heat flux from an oxyacetylene torch their ablation properties could be studied. This is a common method for evaluating preliminary ablative properties for materials and for example used by reference [21] and [22]. Even if the heat flux might be similar to the one in a combustion chamber one must remember that the ablation process is dependent on pressure, chemical composition of the flame, flow velocity and chamber geometry. For those reasons this test can't be used to direct the final design but only tell which materials that are worth investigating deeper by comparing the different materials to each other.

4.1 Experiment set-up

Eight materials where chosen to be tested based on their availability and price. See table 2. Mostly pure polymers but also reinforced with glass and carbon fiber. The test standard ASTM E285 was used but there was not enough time or money to follow the standard completely.

Table 2. Materials that were investigated during the oxyacetylene test campaign.

Material	**Density [kg/m³]**
ABS	1080
Acrylate	1380
Carbon fiber/Epoxy	1330
Glass fiber/Epoxy	2010
Polyamide 6	1230
Polyethylene	1040
Polystyrene	1130
PVC	1620

The test specimen was 2 mm thick and was put in a steel holder that exposed 80x80 mm of the sample to the flame. The oxyacetylene torch was places orthogonal to the sample 19 mm from the surface. A thermocouple was mounted on a graphite rod and by the means of a spring pushed against the back side of the sample aligned with the torch to measure the temperature of the sample. See figure 8, 9 and 10. The sampling rate was 5 Hz. The sample was exposed to the flame until burn-through could be seen. The time was measured and the temperature logged.

The gas flow was supposed to be 6.37 m^3/h with a volume ratio of oxygen to acetylene of 1.20. The mixture would give a chemically neutral flame which was desired since an excess of oxygen would dramatically increase the ablation rate and make the test less realistic since the rocket fuel what is to be used in the booster will have a deficit of oxygen. The desired gas flow could not be achieved simply because there was no flow meter on the torch. Instead the flame could only be adjusted from visual inspection to have a neutral and concentrated flame around 8 mm long. The flame was adjusted on the gas cylinder valves and the valves on the torch where used only for start and stop. By doing this the same flame could be achieved for all tests during one day but the valves had to be closed during the night which introduced an unknown flame difference between different test days. This will be discussed later.

Equipment

- Precioso Loosco cutting torch
- K-type thermocouple
- Dataq DI-710 data logger
- Sample holder

The things in the test standard that were not followed:

- No mass flow measurements. This excluded measurements such as: flow meter, temperature of the flowing gas and pressure before combustion. This made the gas flow and the ratio between oxygen and acetylene unknown which also affects the chemistry of the flame.
- No calorimeter used. This made the exact heat flux unknown.
- Thinner samples. The proper thickness is 6.35 mm but instead samples of 2 mm were used because of availability reasons.

The effects of these changes are discussed in the result section.

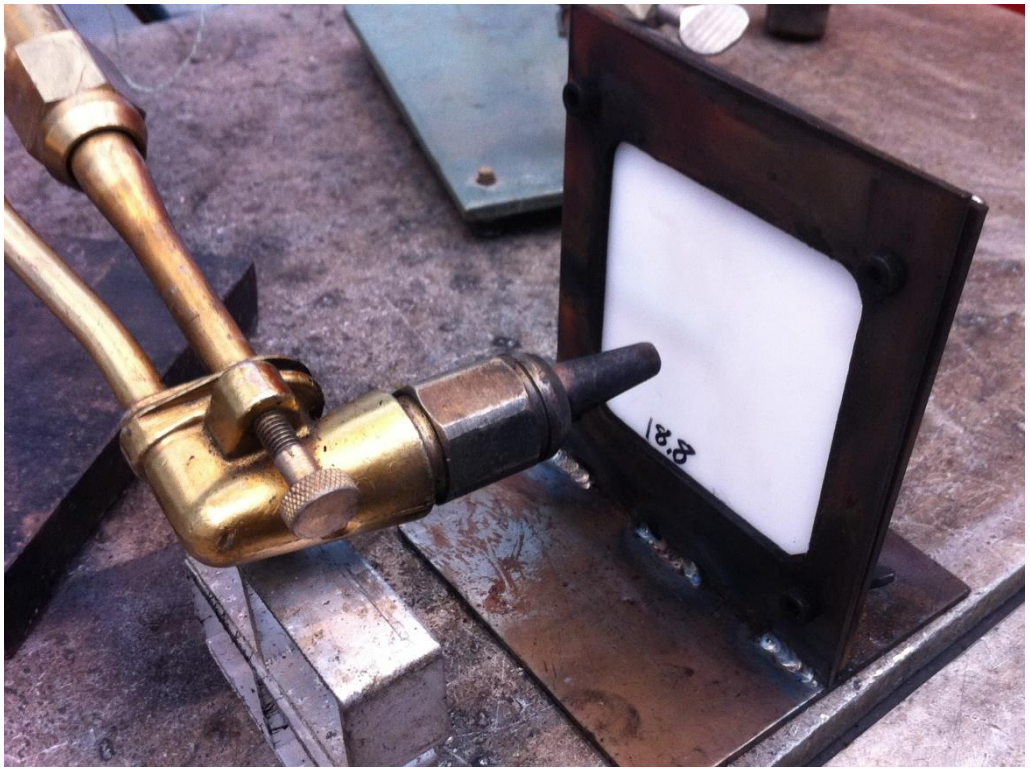

Figure 6: Oxyacetylen torch aimed at sample

Figure 7: Thermocouple held by graphite rod mounted on a spring touching the back side of the sample

Figure 8: Picture from behind during test

4.2 Results

What could be seen from the test was that the non-reinforced materials performed poor, 5-8 s before burn-through could be seen, meanwhile the fiber reinforced materials lasted at least 23 s.

The carbon fiber material performed best when it came to burn through time. It took over 100 s before all the fibers where consumed but the back side of the material self-ignited after only 23 seconds when the thermocouple measured 200°. The epoxy evaporated and left the fibers which are without structural integrity on their own. The temperature rose drastically when the epoxy was gone.

The glass fiber sample lasted long and had the best insulation index, I_T .

$$I_T = \frac{t_T}{d} \tag{15}$$

Where t_T is the time measured for a certain temperature rise, in this case 80° or 180°, and d is the thickness of the sample. It seems like the samples had some kind of fire retardant since it didn't catch fire on the back side as the carbon fiber sample did. This introduced an unknown parameter since no precise data could be found about the material. This were investigated more in the sub-scale motor test campaign.

The deviations from the test standard did effect the results. For example, three of the glass fiber samples were tested the first day of the test campaign and the forth on the second day. The flame composition could not be verified and it seems like there was a significant difference in chemistry or heat flux since the last sample lasted more than four times longer that the three first. This anomaly could of course be disturbing but it didn't change the outcome of the test since this test was done only to sort out the obviously poor materials and all fiberglass samples performed well. The thinner thickness of the samples should not affect the outcome too much especially since 2 mm is closer to the intended thickness of the insulator than 6.35 mm. Fiberglass and carbon fiber were chosen to be investigated further. The results from the test can be found in table 3.

Table 3: Oxyacetylene test results.
$I_{T80°}$ - Insulation Index. The delay per mm for 80° temperature rise.

Material	# of tests	Burn through time [s]	Ablations rate [mm/s]	Ablation rate [s/mm]	Density [kg/m3]	Ablation mass flow [kg/(m2*s)]	$I_{T80°}$ [s/mm]	$I_{T180°}$ [s/mm]
ABS	4	7,35	0,27	3,68	1080	0,29	No data*	
Acrylate	5	8,12	0,25	4,06	1380	0,34	No data*	
Carbon/Epoxy	2	104	0,02	52,36	1330	0,03	3,5	7,3
Glass/Epoxy	4	23 – 98	0,02 - 0,09	11 – 50	2010	0,04 - 0,18	4,1	11,5
Polyamide 6	5	6,24	0,32	3,12	1230	0,39	No data*	
Polyethylene	5	5,8	0,34	2,9	1040	0,36	No data*	
Polystyrene	5	4,6	0,43	2,3	1130	0,49	No data*	
PVC	5	4,7	0,43	2,35	1620	0,69	No data*	

* The non-reinforced materials had burn through before the thermocouple could detect 80° temperature rise.

5 Motor Test

Since the oxyacetylene torch test does not represent the final conditions when it comes to heat, pressure, chemical composition and flow velocity a test motor was built based on a fuel very similar to the one that is to be used in the DART booster. This gave an opportunity to study the ablation rate under more realistic conditions in respect to temperature and flow velocity where the pressure could be altered so the ablation's pressure dependence could be studied. It was expected that it would be difficult to achieve a pressure of 7 MPa in the test motor which is the target pressure of the booster. The goal of the test where therefor to find out the pressure dependence according to equation (2) under the assumption of constant temperature and flow velocity to be able to extrapolate the results and estimate the ablation rate at 7 MPa.

5.1 Experiment set-up

A sub-scale test engine was built, figure 11, 12 and 13, which could be loaded with different propellant geometries to be able to alter the burn profile and the steel nozzle had a graphite insert which could be exchanged to achieve different pressures. A Dataq DI-710 was used to log the pressure data at 200 Hz. The propellant were White Lightning from Aerotech which has many similarities with the fuel that will be used in the booster. 20-60 g were used in each firing. All tests were video recorded.

The test materials were delivered from Futura Composites in the Netherlands which will manufacture the casing for the booster. Unfortunately they did not want to specify any information about the materials except density and fiber fraction for carbon composite.

- Carbon fiber/epoxy (Carbon)
  - Unidirectional
  - 1560 kg/m^3
  - 65 % fiber fraction by volume
- Glass fiber/epoxy (Glass)
  - 0/90 woven fabric
  - 2000 kg/m^3
- Glass fiber/epoxy/alumina (Glass FR)
  - 0/90 woven fabric
  - 2000 kg/m^3
  - Alumina as fire retardant, amount was classified

Only six firings could be done due to a limited amount of propellant and test material. Three samples could be placed in the test motor so each firing had one of each material. The specimens were fastened with M3 screws in a holder of steel and the screw holes were filled with silicon glue to protect the screws from the heat. There were a gas deflector made from graphite between the propellant and the specimens to protect specimens from direct flow on the side perpendicular to the flow. Excess axial space were filled up with wood behind the propellant when needed. See figure 11.

The test plan was to fire the motor two times at three different pressures aiming for a burn time around 5 s. See table 4. What made the situation complicated was that almost no data regarding the propellants burn characteristics could be found. Since the pressure was difficult to estimate for the first motor configuration a very low combustion pressure were used for the first two firings for safety reasons. These data points are the least interesting since it is desirable to have data points as close to the target pressure as possible. As the propellant properties were found the combustion pressure could be increased. Although 70 bars could not be achieved with the sub-scale motor due to the fact that the nozzle would have been very small. If a solid piece from the specimens would get loos it could block the nozzle which could lead to a pressure rise and a rapid unexpected motor disassembly.

Table 4. Test matrix.

Test	Pressure	Material tested
Firing 1	Pressure # 1	One of each material tested
Firing 2	Pressure # 1	One of each material tested
Firing 3	Pressure # 2	One of each material tested
Firing 4	Pressure # 2	One of each material tested
Firing 5	Pressure # 3	One of each material tested
Firing 6	Pressure # 3	One of each material tested

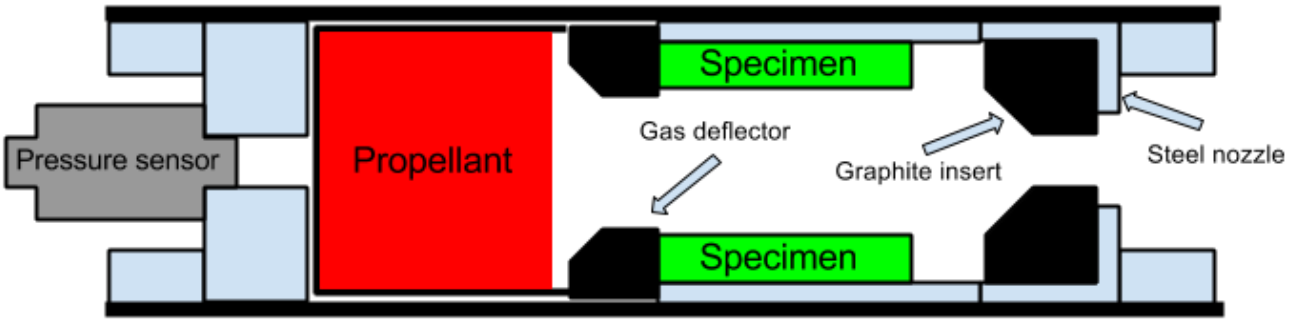

Figure 9: Schematics of the sub-scale test motor

Figure 10: Interior motor parts laid up next to casing

Figure 11. Material specimens mounted in the holder.

5.2 Results

Six firings of the sub-scale test motor were conducted. A problem that arose was that ash from the fuel settled on the nozzle walls and made the diameter 0.15-0.3 mm smaller. This increased the klemmung value, which is the area ratio between the exposed propellant and nozzle throat, and hence also the combustion pressure. This phenomenon limited the possibility of reaching higher pressures since a very small nozzle risked to be fully blocked. It also made the measurements difficult since the pressure was not constant during the burn. The ablation pressure dependence is for that reason based on the average pressure of each burn. The results are also based on the assumption that the regression is linear with time. That is consistent with the Q^* analysis and the char-erosion-rate analysis in reference [14] but not consistent with reference [23] which treat ablation in the nozzle region. Both reports are from NASA published only one year apart.

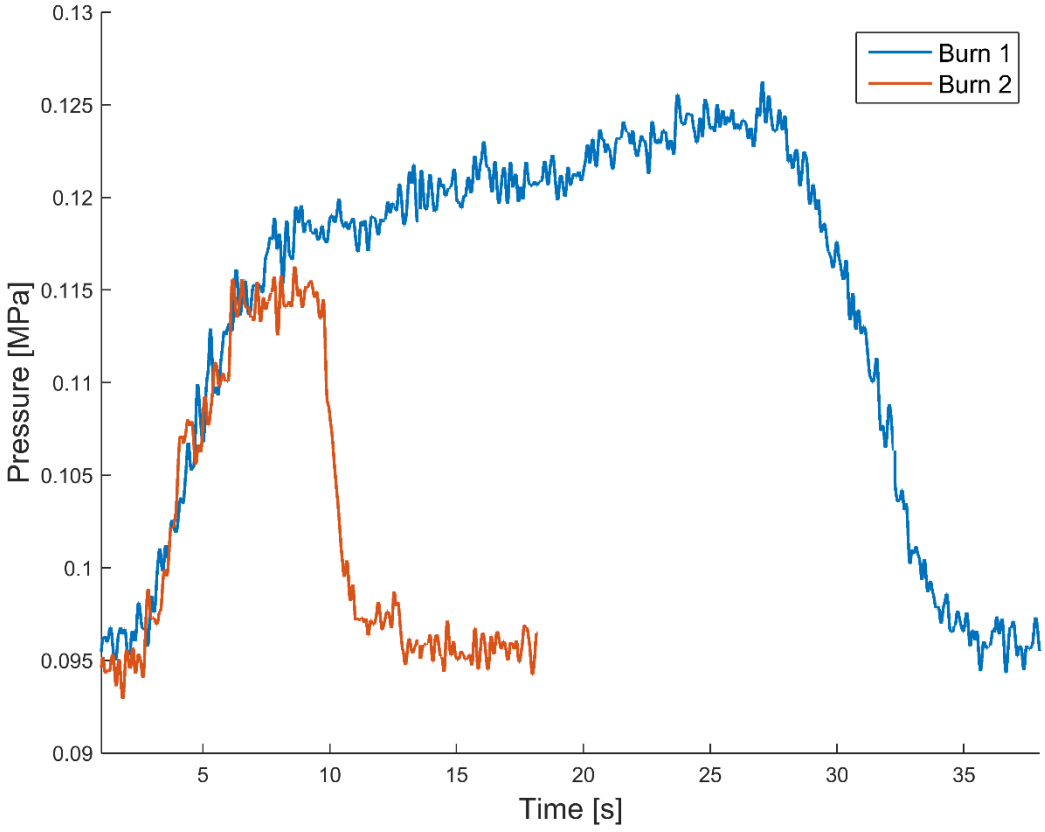

Figure 12: Pressure curve for burn 1 and 2

The first two burns had a klemmung of 36. This is very low and was chosen because the burn rate and burn rate exponent of the fuel were unknown. The pressure rice was only 25 kPa, see figure 14, and the nozzle flow was even subsonic. The first burn duration was 28 s. For the second test the fuel grain was adapted to have a duration in the range of 5 s like the DART booster will have.

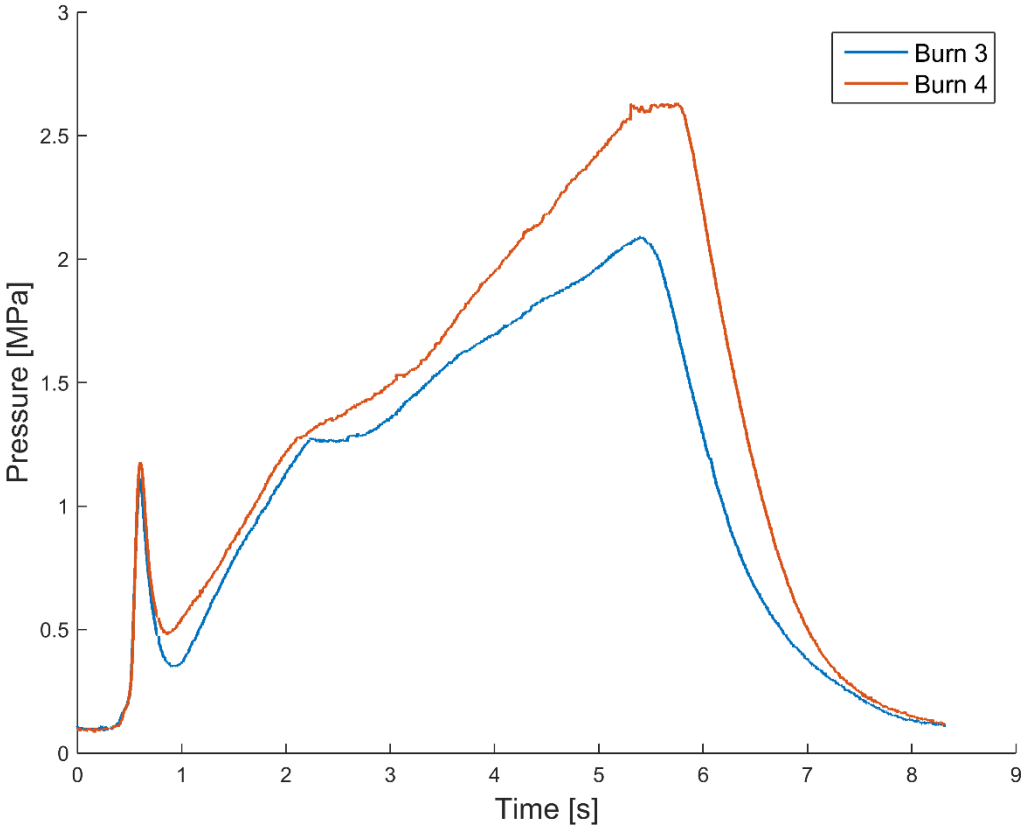

Figure 13: Pressure curve for burn 3 and 4

During burn 3 and 4 the clogging of the nozzle became a real problem. The first sharp peak in figure 15 is the ignition charge and stable burning seems to be achieved after two seconds. Then the nozzle diameter gradually changed from 2.8 to 2.5 mm. The klemmung went from 198 to 248. The fourth burn was planned to have a 25 % longer burn time but for some reason the pressure became slightly higher which resulted in higher burn rate and the burn time remained almost constant.

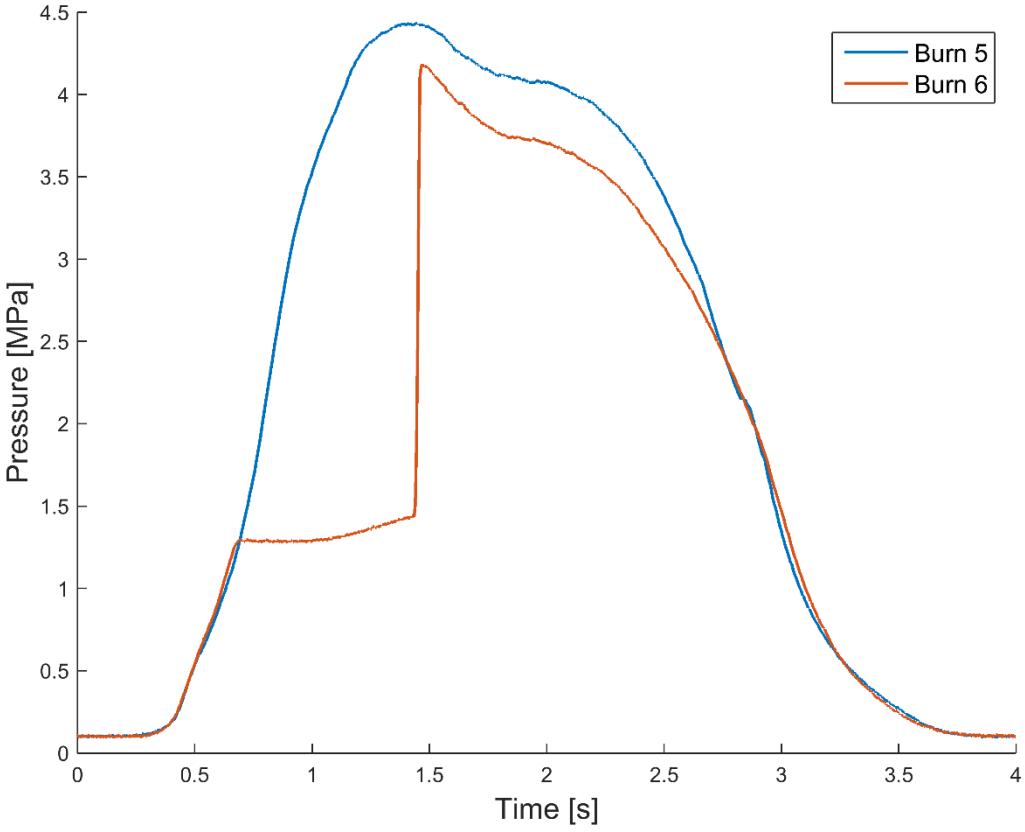

Figure 14: Pressure curve for burn 5 and 6

The results from burn 5 and 6 can be seen in figure 16. In all previous tests end-burning fuel grains were used but since they have small surface area and the nozzle could not be made smaller the propellant geometry were exchanged for a bates grain with 2.54 times bigger surface area but the burn time was unavoidable made shorter. The peculiar shape of burn 6 is due to a blocked pressure sensor port. That conclusion was made from the facts that the integral of the two curves should be identical and that the disassembled motor showed signs of that a wooden piece had been pushed towards the sensor.

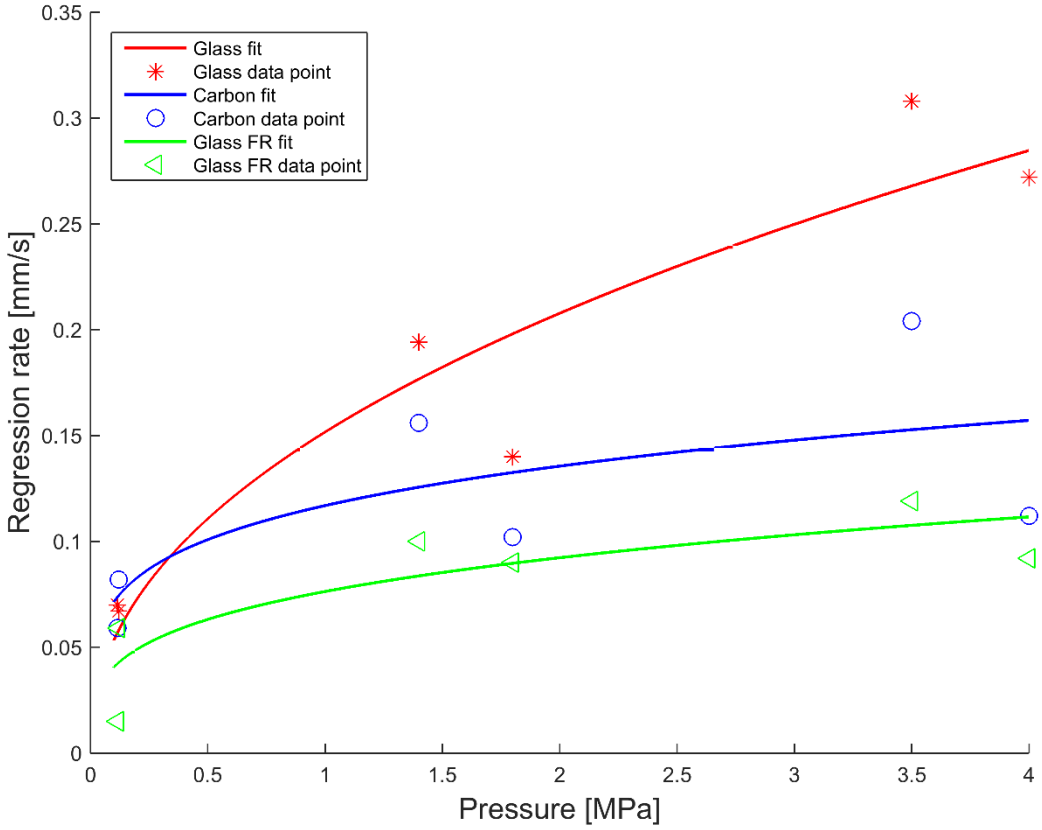

Figure 15: Regression data and fitted curves

The regression of the samples were measured with a caliber. Both glass samples made from 0/90 weave had a plane regression surface which made measurements easy. The unidirectional carbon sample on the other hand often had an uneven surface which made measurements difficult. A mean value from the central regions were used.

The results from the tests can be seen in figure 17. One of the low pressure data points for Glass FR shows a very low regression rate. That one comes from burn number two with low pressure and short duration. The fire retardant used was alumina which form a heat resistant layer of alumina on the material surface in case of fire. It could be the case that this alumina layer produce a transient phenomenon which only can stand minor heat loads for a limited time. How big effect this phenomenon has on the other samples is difficult to say.

The fitted curves in figure 17 comes from equation (2) and are on the form aP^b where a and b are constants. Temperature and flow velocity are assumed to be constant. As can be seen in table 5 the confidence interval are quite big and using any of its extremes would give an insulator either unrealistically thin or disturbingly thick.

Table 5: Model constants and confidence intervals

Material	Constants	95 % confidence interval
Glass	a=0,1516	0,09322 - 0,21
	b=0,4543	0,1256 – 0,783
Glass FR	a=0,0763	0,0491 – 0,1035
	b=0,274	-0,02134 – 0,5693
Carbon	a=0,1169	0,06651 – 0,1673
	b=0,2136	-0,1337 – 0,5609

6 Conclusions

The results of this investigation are not certain but point out a direction in which to proceed the work. The test campaign was very short and really relevant pressures were never achieved. The model used is most reliable when data is collected from similar conditions as the target situation. What this report will do is to give recommendations on future work.

6.1 Summary of results

The regression rate is expressed in equation (2) and if the temperature and flow velocity are assumed to be constant the expression looks like

$$\dot{x} = aP^b \tag{16}$$

And only two constants needs to be found. The temperate is dependent on the fuel and will remain constant. The flow velocity has changed some during the tests but always remained below 10 m/s and the velocity's influence is expected to be far below linear since ablative insulators otherwise would be highly inappropriate for rocket nozzles and atmospheric reentry vehicles where it in fact is frequently used. The low flow velocity will also be true in the booster since the only exposed insulator surface is the small gap between the bates grains where no flow is expected.

The results from an extrapolation of this model can be found in table 6 where the constants comes from MATLAB's function "fit", "power1".

Table 6: Predicted insulator regression and mass

Material	Density [kg/m³]	Regression at 7 MPa, 5 s [mm]	Insulator mass [kg/m²]
Glass	2000	1,84	3,680
Glass FR	2000	0,65	1,300
Carbon	1560	0,89	1,388

6.2 Analysis and interpretation

There is an intrinsic uncertainty in the results since they are based on very few data points. This is not a too big problem, these tests were never meant to deliver the final design but make a path for future work. The real choice is between an insulator made from glass fiber with fire retardant or one from carbon fiber. A thermal safety factor of 100 % or more is common if the ablator is not well characterized. [14] That would give a thickness of 1.3 mm of glass fiber FR or 1.8 mm of carbon fiber. The outside diameter of the booster is determined by the launch rail so the thinner insulator the more propellant can be put in the casing. If the propellant is assumed to have a density of 1800 kg/m^3 and the loadbearing part of the casing has an inner diameter of 110 mm one can see that the Glass FR insulator can house 0,288 kg of extra propellant per m of propellant compared to the Carbon insulator. The mass of the insulators are quite similar but the booster would have a little higher deltaV if Glass FR were used but that would give a casing that would be slightly more complicated to manufacture compared to a pure carbon fiber casing. See table 7.

Table 7: Insulator impact on mass and volume

Material	**Mass of insulator/meter [kg/m]**	**Volume of booster/meter [m^3/m]**
Glass FR	0.847	0.008235
Carbon	0.910	0.008075
Comparison	Glass FR is 0,063 kg lighter	Glass FR is $1.6 \cdot 10^{-4}$ m^3 bigger

6.3 Future work

During the future development of the DART booster a series of single grain and full scale tests will be done. A gap between the grain and the front bulk head can be left to expose the insulator to a realistic heat load, chemistry and pressure at a low flow velocity during the single grain tests. The thermal protection could then be optimized. How much heat that actually will reach the insulator between the bates grains can be studied during the full scale tests but one must bear in mind that if considering the propellant casting tubes and the spacers between the grains as a part of the insulator one risk failure of the motor if an assembly error occurs. This would demand that the propellant grains are bound to the casing since the propellant otherwise would sink to the bottom of the combustion chamber due to the high acceleration and expose the top of the insulator. Either way, bonding the propellant grains to the casing would be beneficial from a heat load perspective but also from a vehicle stability perspective since the center of gravity would travel towards the tail if the propellant moves which could compromise the stability.

It would be interesting to see how the carbon fiber would perform with added fire retardant. Futura Composites had no experience of that combination and had no samples to give. That could be an area of future investigation.

References

[1] "NASA Sounding Rockets, 1958-1968: A Historical Summary, Ch. 2". NASA. 1971.

[2] W. A. P. Martin (1901). "The Lore of Cathay or The Intellect of China", New York: Fleming H. Revell Company, p. 25

[3] Crosby, Alfred W. (2002). "Throwing Fire: Projectile Technology Through History." Cambridge: Cambridge University Press. pp. 100–103. ISBN 0-521-79158-8.

[4] Goddard, Robert (2002). "Rockets", New York: Dover Publications, ISBN 978 0-486-42537-5

[5] J. D.Hunely. 1999. "The history of solid propellant rocketry: what we do and do not know", NASA Dryden Flight Research Center Edwards, California

[6] P. G. Hill, C. R. Peterson. 1992. "Mechanics and Thermodynamics of Propulsion." Second edition, pp. 590.

[7] Diebold, James P. (17 April 1973). "Encapsulation of Nitronium Perchlorate Employing Ammonia to Form Ammonium Perchlorate." (Patent) Department of the Navy, Washington DC. Accession Number: AD0164909.

[8] C. Song, P. Wang, H. A. Makse. 29 May 2008. "A phase diagram for jammed matter". Nature 453 (7195): 629-632.

[9] Alain Davenas. 1993. "Solid Rocket Propulsion Technology", chapter 2.

[10] R. Geisler C. Beckman. 1998. "The History of the BATES Motors at the Air Force Rocket Propulsion Laboratory. " Air Force Research Laboratory. AIAA-98-3981.

[11] P. G. Hill, C. R. Peterson. 1992. "Mechanics and Thermodynamics of Propulsion." Second edition, pp. 618.

[12] M. Q. Brewster. 1989. "Radiation-stagnation flow model aluminized solid rocket motor internal insulator heat transfer", Journal of Thermophysics and Heat Transfer, Vol. 3, No. 2 (), pp. 132-139.

[13] F. C. Price, V. A. Marple, R. A. Dupuis. 1964. "Internal environment of solid rocket nozzles" Philco, Ford Motor Company Research Laboratories.

[14] Howard W. Douglass, Sherwood E. Twitchell. 1976. "Solid rocket motor internal insulation". Lewis Research Center, NASA.

[15] Thermopedia – Ablation. Avalable from: <http://www.thermopedia.com/content/285/>. [1 October 2015]

[16] Thermopedia – Transpiration Cooling. Avalable from: <http://www.thermopedia.com/content/1203/>. [1 October 2015]

[17] Thermopedia – Film Cooling. Avalable from: <http://www.thermopedia.com/content/759/>. [1 October 2015]

[18] J. Östlund. 2015. "Thrust Chambers", MJ2246 Rocket Propulsion, Lecture at Royal Institute of Technology. 5 February.

[19] Brookley, C.E. 1963. "Measurement of Heat Flux in Solid Propellant Rocketry." Allegany Ballistics Laboratory, ABL/Z-60(AD-432472).

[20] Y. Fabignon. 1993. "Ablation Rate Calculation of Thermal Insulations in Segmented Solid Propellant Rocket Motors." Office National d'Etudes et de Recherches Aérospatiales, AIAA 93-1884. Pp 5.

[21] E. L. Corral, L. S. Walker. 2010. "Improved ablation resistance of C-C composites using zirconium diboride and boron carbide." Arizona Materials Laboratory, Materials Science and Engineering Department, The University of Arizona.

[22] G. Pulica, J. Tirillo, F. Marra, F. Fossati, C. Bartuli, T. Valente. 2010."Carbon-phenolic ablative materials for re-entry vehicles: Manufacturing and properties." Dept. of Chemical Engineering, Materials, Environment, Sapienza University of Rome.

[23] J. H. Collins. 1975. "Solid Rocket Motor Nozzles." Lewis Research Center, NASA. Pp 51.

7 Appendix

Appendix A: Test motor log

7.1 Appendix A

Test Motor 1

Lenght of fuel [mm]	40
Mass of fuel [g]	92,16
Nozzle diameter [mm]	6,5
Klemmung	36,8
Burn time [s]	28
Pressure (absolut) [MPa]	0,12

Results	Thickness before test [mm]	Thickness after, with char [mm]	Remaining fresh material [s]	Regression [mm]	Regression rate [mm/s]
Glass	10,600	13,120	8,730	1,870	0,067
Glass FR	8,400	9,000	6,750	1,650	0,059
Carbon	8,800	9,300	6,500	2,300	0,082

Test Motor 2

Lenght of fuel [mm]	8,5
Mass of fuel [g]	19,584
Nozzle diameter [mm]	6,6
Klemmung	35,7
Burn time [s]	8
Pressure (absolut) [Mpa]	0,115

Results	Thickness before test [mm]	Thickness after, with char [mm]	Remaining fresh material [s]	Regression [mm]	Regression rate [mm/s]
Glass	12,380	12,840	11,820	0,560	0,070
Glass FR	8,320	8,620	8,200	0,120	0,015
Carbon	8,830	9,190	8,360	0,470	0,059

Test Motor 3

Lenght of fuel [mm]	20
Mass of fuel [g]	46,08
Nozzle diameter, start [mm]	2,8
Nozzle diameter, end [mm]	2,5
Klemmung, start	198
Klemmung, end	248
Burn time [s]	5
Pressure (absolut, average) [MPa]	1,4

Results	Thickness before test [mm]	Thickness after, with char [mm]	Remaining fresh material [s]	Regression [mm]	Regression rate [mm/s]
Glass	11,870	-	10,900	0,970	0,194
Glass FR	8,370	-	7,870	0,500	0,100
Carbon	8,580	-	7,800	0,780	0,156

Test Motor 4

Lenght of fuel [mm]	25
Mass of fuel [g]	57,6
Nozzle diameter, start [mm]	2,8
Nozzle diameter, end [mm]	2,6
Klemmung, start	198
Klemmung, end	230
Burn time [s]	5
Pressure (absolut, average) [MPa]	1,8

Results	Thickness before test [mm]	Thickness after, with char [mm]	Remaining fresh material [s]	Regression [mm]	Regression rate [mm/s]
Glass	12,390	13,350	11,690	0,700	0,140
Glass FR	8,260	8,550	7,810	0,450	0,090
Carbon	8,960	9,530	8,450	0,510	0,102

Test Motor 5

Lenght of fuel [mm]	BATES	OD=33,2 ID=10 L=48,5
Mass of fuel [g]	61	
Nozzle diameter, start [mm]	3,25	
Nozzle diameter, end [mm]	3,05	
Klemmung, start	373	
Klemmung, end		
Burn time [s]	2,5	
Pressure (absolut, average) [MPa]	4,0	

Results	Thickness before test [mm]	Thickness after, with char [mm]	Remaining fresh material [s]	Regression [mm]	Regression rate [mm/s]
Glass	12,070	12,400	11,390	0,680	0,272
Glass FR	8,000	7,970	7,770	0,230	0,092
Carbon	7,740	7,460	7,460	0,280	0,112

Test Motor 6

Lenght of fuel [mm]	BATES		OD=33,2 ID=10 L=48,5
Mass of fuel [g]		61	
Nozzle diameter, start [mm]		3,25	
Nozzle diameter, end [mm]		3,01	
Klemmung, start		373	
Klemmung, end			
Burn time [s]		2,6	
Pressure (absolut, average) [MPa]		3,5	

Results	Thickness before test [mm]	Thickness after, with char [mm]	Remaining fresh material [s]	Regression [mm]	Regression rate [mm/s]
Glass	12,600	13,100	11,800	0,800	0,308
Glass FR	8,380	8,350	8,070	0,310	0,119
Carbon	8,210	8,500	7,680	0,530	0,204